JOURNAL OF AIRCRAFT
Vol. 45, No. 2, March–April 2008

High-Order Finite Elements for Structural Dynamics Applications

Paolo Lisandrin* and Michel van Tooren†
Delft University of Technology, 2629 HS Delft, The Netherlands

DOI: 10.2514/1.26498

In this paper a new "element independent" finite-element modelling and analysis method for the efficient modal analysis of structural elements is presented. At the core of this method is the use of a single, high-order (*p* formulation), brick-type finite element for modeling one-, two-, and three-dimensional-like structural elements. The use of a single element guarantees speed and flexibility in the (re)modeling of the structure and solves the consistency and the convergence problems connected to finite-element analysis in preliminary design. The performance of this approach is evaluated on the modal analysis of unconstrained panels made of an isotropic material and having different thicknesses and different curvatures. Comparison with results from traditional linear shell finite-element models shows that, with the new method, in most of the cases analyzed, accurate results can be obtained with fewer degrees of freedom. In the worst cases the results are comparable (in terms of convergence rate and number of degrees of freedom needed to calculate a converged solution) with those obtained from shell linear models.

I. Introduction

IN THE preliminary phase of the design cycle, the frequent changes in the geometrical, conceptual, and physical properties of the configuration and the lack of experimental data challenge the design team to keep the models used for design up to date.

Changes in geometry and material, for example, directly affect the finite-element (FE) modelling. As a result, a large amount of time is spent preparing, modifying, and updating the models to follow modifications in the design. These operations, very time consuming and normally performed by hand, restrict the time dedicated to the design phase. Therefore, a fast and flexible way of modifying the properties of the design is crucial.

Furthermore, the ability to predict with high accuracy and limited computational cost the properties of different design concepts is fundamental for the success of the project, both in terms of meeting its requirements and reducing the operating costs. For example, errors in the evaluation of the flutter speed in the preliminary design phase that are recognized only when experimental data from ground vibration, flight, wind-tunnel tests become available, can lead either to an expensive redesign of the complete concept or the introduction of major modifications, like weight penalties or flight envelope limitations, of the final configuration. The possibility of using a fast and accurate numerical tool is the solution for limiting the uncertainties in the preliminary design phase.

One fundamental step in the determination of the flutter speed of an aircraft is the calculation of the modal shapes and the natural frequencies. The current approach followed in the industry for the determination of the modes is to derive reduced models, based on beam finite elements and lumped masses conveniently placed, from a very detailed FE model. Each time a modification is introduced in the properties of the configuration analyzed, new reduced models must be generated and the reduction process is neither straightforward nor simple.

Received 12 July 2006; accepted for publication 30 October 2007.

*Ph.D. Student, Faculty of Aerospace Engineering, Kluyverweg 1; P.Lisandrin@tudelft.nl. Member AIAA.

†Full Professor, Faculty of Aerospace Engineering, Kluyverweg 1; M.J.L.vanTooren@tudelft.nl.

The goal of the FE modeling approach proposed in this paper is to provide a tool capable of the following: 1) a complete automatic FE meshing and (fully converged) analysis, limiting to a minimum the interaction with the user; and 2) the calculation of fast and accurate solutions that make use of a full model, thereby overcoming further approximation introduced by the use of beam reduced models.

To understand how to achieve these goals, we should consider the two main problems faced by an automatic mesh generator when an FE model is created: the consistency and the convergence of the model.

Consistency is related to the type of finite element to be used for modeling a certain structural part. An FE code provides a wide choice of elements, any of them having their own field of application and limits. Each of them is guaranteed to be optimal for certain applications and is suitable for modeling specific structural parts. An experienced FE analyst knows where to place a certain kind of element and why. An automatic mesher should be able to do the same or circumvent the problem. An ideal approach would be the use of a "general" element, capable of representing the behavior of one-, two-, and three-dimensional structural elements.

Convergence of the model is related to the choice of the number of elements necessary to achieve the required degree of accuracy of the solution. In the current practice the acceptance of convergence is left to experienced people, but in an automatic mesh generator/analysis tool, where every decision is rule based, there should be a criterion to define this number. In theory, a convergence analysis should be performed to determine the right number of elements to be used, for example increasing the number of elements within the structural component. This is not an efficient approach when dealing with the mesh of a complete aircraft in the preliminary design phase. The solution could be the use of elements guaranteed to have a high rate of convergence as well as an easier approach in the convergence verification.

A solution to the problems of consistency and convergence can be found in the use of finite elements based on higher order shape functions, specifically in the form of "*p*-formulation" and "brick" finite-element types.

P-formulation finite elements were introduced by Babuska et al. [1]. For this class of finite elements, convergence is achieved by increasing the polynomial order of the shape functions, built through the use of hierarchical polynomials [1], such that every time the order of a polynomial is increased, new degrees of freedom are added.

The first advantage of the proposed approach stems from the use of a brick-type finite element based on a fully three-dimensional formulation for the displacement field. The lack of any a priori assumptions on the kinematics or the geometry of the structure, in

contrast with formulations based on thin plate theory [2], makes this element suitable for representing any kind of structural part, that is, both thin and thick shells and beams [3]. Therefore, only one kind of finite element can be used to model and analyze a complete structure, with the potential of bringing a major improvement in speed and flexibility to the first modeling phase of the structural analysis or when modifications in the structural model are introduced and a new FE model must be generated.

Another advantage of the present approach comes from the use of a finite element based on high-order shape functions in the form of the p formulation. It is known that, with the commonly used linear interpolation shape functions, locking phenomenon [4–6] can occur. It is due to the inability of the lower order shape functions to correctly interpolate the displacement field, leading to an overestimation of the stiffness of the element. Several remedies, such as selective and reduced integration, incompatible modes, and assumed strains [7], are implemented in commercial finite-element codes to avoid locking. In the present work, the use of high-order shape functions directly eliminates the occurrence of this phenomenon without recurring to any numerical treatment.

A further advantage stems from the fact that in the p elements the order of the shape function is not fixed; it can be varied in principle to any value. Adaptive analyses can be performed, deciding a starting order for the polynomials to be used and increasing it until a certain convergence criterion has been satisfied or when a maximum polynomial order has been reached. Convergence checks on complex structures such as a whole aircraft become feasible, whereas by using common linear elements, or using other higher order formulations where the order of the polynomial is fixed, like in Morino et al. [8], this would not be possible without regenerating the complete mesh several times. It is industry practice to generate just one final mesh with the number of elements defined a priori by experienced people, or, especially for modal analyses, reduced models made of beams and lumped masses are created. These models are not always affordable, especially in structures made of composite materials where the reduction process is even more difficult. P-formulation elements make the convergence check process easily automatable and this is particularly important in the preliminary design/multidisciplinary optimization environment, where no experimental data are available and product properties derivation relies heavily on numerical calculations.

II. NASTRAN Implementation of *P* Elements

The commercial finite-element package NASTRAN [9] offers the possibility of using the p elements in performing both static and normal modes analyses. Convergence of a solution can be achieved by reducing the elements' size (referred to as h convergence) or increasing the polynomial order of the shape functions (referred to as p convergence).

Adaptive analysis can be performed by varying the polynomial order of the shape functions independently in each element, and for each element varying the order along each of the three directions of its natural coordinate system independently. The user can select for each finite element or for a group of finite elements a minimum and a maximum polynomial order for the shape functions for any of the directions of the natural coordinate system. A first solution is calculated using the minimum polynomial order, and then the error of the solution is estimated using stress discontinuity and strain energy sensitivity methods [10,11].

Depending on the error estimation, the polynomial order is increased independently on each local direction and for each element autonomously. A new solution is calculated and a new error is estimated. The process stops when the error for each element is below a threshold value input by the user or when a maximum number of computational steps has been reached. The adaptive analysis has the advantage of being fully automated, as only one mesh is needed and the changing of the polynomial orders is performed internally, offering the possibility to automate the analysis process.

III. Modal Analysis of Flat Plates

The determination of the modes and the frequencies of a structure requires the solution of the classical free vibration equations:

$$\mathbf{M}\ddot{\mathbf{u}} + \mathbf{K}\mathbf{u} = 0 \tag{1}$$

where $\mathbf{M}$ is the mass matrix, $\mathbf{K}$ is the stiffness matrix, and $\mathbf{u}$ is the displacement field. In the frequency domain, Eq. (1) can be rewritten in the form

$$-\omega^2\mathbf{M}\tilde{\mathbf{u}} + \mathbf{K}\tilde{\mathbf{u}} = 0 \tag{2}$$

known as the *generalized eigenvalue problem*, where $\tilde{\mathbf{u}}$ is the Fourier transform of the displacement vector $\mathbf{u} = \mathbf{u}(\mathbf{x}, t)$. To keep the problem as general as possible, it is convenient to make the system nondimensional with respect to some material properties, considered isotropic, like the Young's modulus E and the density ρ. The system (2) can be rewritten in the following form [12]

$$-\hat{\omega}^2\hat{\mathbf{M}}\tilde{\mathbf{u}} + \hat{\mathbf{K}}\tilde{\mathbf{u}} = 0 \tag{3}$$

$$\tilde{\mathbf{v}} = \frac{\tilde{\mathbf{u}}}{L}, \qquad \hat{\omega}^2 = \omega^2\frac{\rho}{E}, \qquad \hat{\mathbf{M}} = \frac{\mathbf{M}}{\rho}, \qquad \hat{\mathbf{K}} = \frac{\mathbf{K}}{E} \tag{4}$$

The nondimensionalization has been performed in NASTRAN, setting $E = 10^6$ (this high value has been chosen to avoid numerical problems with frequencies that are too small), $\rho = 1$, and the Poisson number to $\nu = 0.225$, equal to the one of the aluminum alloys.

In this section, a modal analysis of an unconstrained flat, square plate of isotropic material having different aspect ratios (defined as the ratio between the side length of the square plate and the thickness) is performed. The plate is modeled using solid brick elements with p formulation (CHEXA) and four noded linear shell elements (CQUAD4). Both finite-element models use a consistent formulation for the mass matrix. The convergence histories of the natural frequencies versus the number of degrees of freedom are evaluated. Results are presented up to the eighth nonrigid mode. The modes are named according to the corresponding frequency, in ascending order, so that the first mode corresponds to the lowest (nonzero) frequency. The frequencies' results are truncated to the third significative digit. From a purely mathematical standpoint, all significative digits should be retained in the presentation of the results but, for the purposes of a preliminary design environment, a few digits can be acceptable for evaluating the convergence of a computation.

A. Thick Plate

The plate analyzed has dimensions of $L_1 \times L_2 \times L_3 = 1 \times 1 \times 0.01$, Fig. 1. According to the classical plate theory [2], a plate with such a thickness is referred as a "thin" plate, with all the deductions coming from such a hypothesis. Unlike the classical theory, this plate is referred to as thick, as its thickness is of the order of a centimeter, thus 1 order of magnitude higher than the thickness of a typical aeronautical panel, whose thickness is of the order of millimeters.

When the plate is meshed using solids, the number of elements along the thickness must be specified. As the thickness is "small" compared with the in-plane dimensions of the plate, this should imply that less elements are needed along the thickness. To investigate this aspect, a sensitivity analysis has been done on the

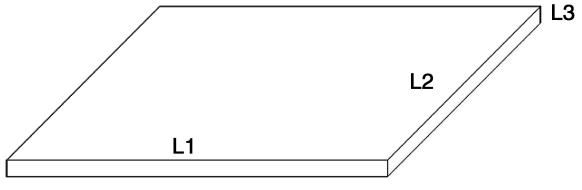

Fig. 1 Flat plate geometrical parameters.

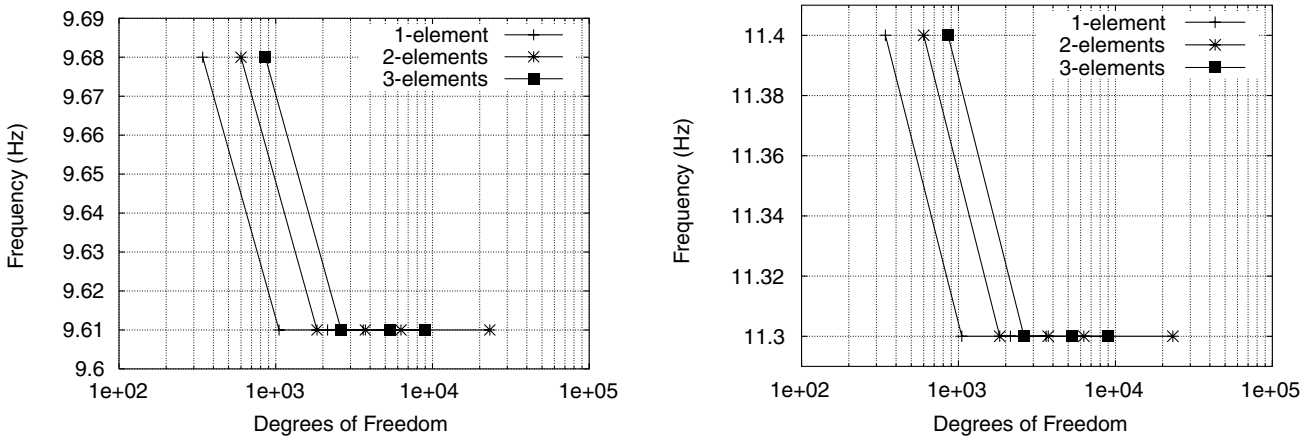

a) Second mode **b) Third mode**

Fig. 2 Sensitivity analysis for the number of elements along the thickness.

effect of the number of elements chosen for the mesh along the thickness on the calculated natural frequencies. For this sensitivity analysis, the polynomial order of the p elements has been kept fixed and the convergence has been checked, just increasing the number of elements in the in-plane directions and keeping fixed the number of elements along the thickness. Figure 2 shows the trend of the second and third frequencies versus the number of degrees of freedom of the model for one, two, and three elements along the thickness. As can be seen, the solution does not depend at all on this number; thus, in the following calculation only one element will be put along the thickness of the plate.

In addition, the p formulation allows the choice of the polynomial order of the shape functions along the three edges of a solid element. Because of the small thickness of the plate, the solution is expected not to be sensitive to the choice of the polynomial order along the thickness provided that it is high enough to prevent locking of the element. Thus, a sensitivity analysis on the choice of the order of the polynomials along the element thickness has been performed.

Figure 3 shows the trend of the second and third frequencies versus the number of degrees of freedom of the system considering three different choices for the shape functions order: fifth order for the two in-plane directions and fifth, third, and second order along the thickness, labeled respectively brick-p5, brick-p553, and brick-p552. The figure shows that when the order of the polynomials along the thickness is lowered, the solution is not affected at all, that is, the curves are shifted on the left-hand side, which indicates a reduction in the size of the system, thus, a reduction in the computational time.

Following these results, the calculations performed with the solid p elements have been done with one element and second-order polynomials along the thickness.

A convergence analysis of the natural frequencies of the square plate has been performed for both the shell and solid models, by increasing the number of elements along the in-plane edges, that is, in the *standard* way (*h convergence*). The mode shapes of the first eight modes are shown in Fig. 4. For the solid model, based on p elements, the choice of the polynomial order is free.

Three different orders have been selected for the in-plane edges, in particular, third, fifth, and seventh, resulting in three solid models. These models are referred to in the figures as brick-p332, brick-p552, brick-p772.

Figures 5 and 6 represent the frequencies versus the number of degrees of freedom. The meshes selected start at one element per edge and go up to the number of elements at which convergence is achieved. The result is considered converged when the last three runs give the same result (first three significative digits coincident) for the frequencies. In Fig. 5, the result obtained using one element for the case brick-p332 has been removed as it was off by more than 20% from the converged result.

Figures 5 and 6 show that, depending on the polynomial order chosen, the solid model is able to behave exactly as the shell model as converged values are the same except for the first, sixth, and eighth mode for which the shell model predicts a converged value slightly different from the solid models (the difference is at the third decimal digit). The first five mode shapes define the "base"-type plate vibrations. The remaining mode shapes (six–eight) are the higher

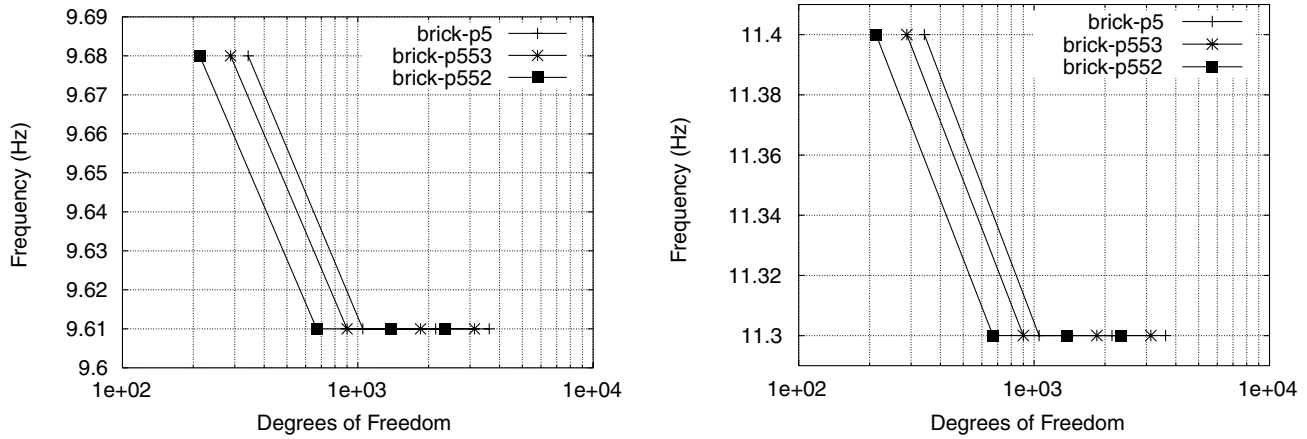

a) Second mode **b) Third mode**

Fig. 3 Sensitivity analysis for the polynomial order choice along the thickness. Thick plate, $L_1 = 1$, $L_2 = 1$, an d$L_3 = 0.01$; one element along the thickness.

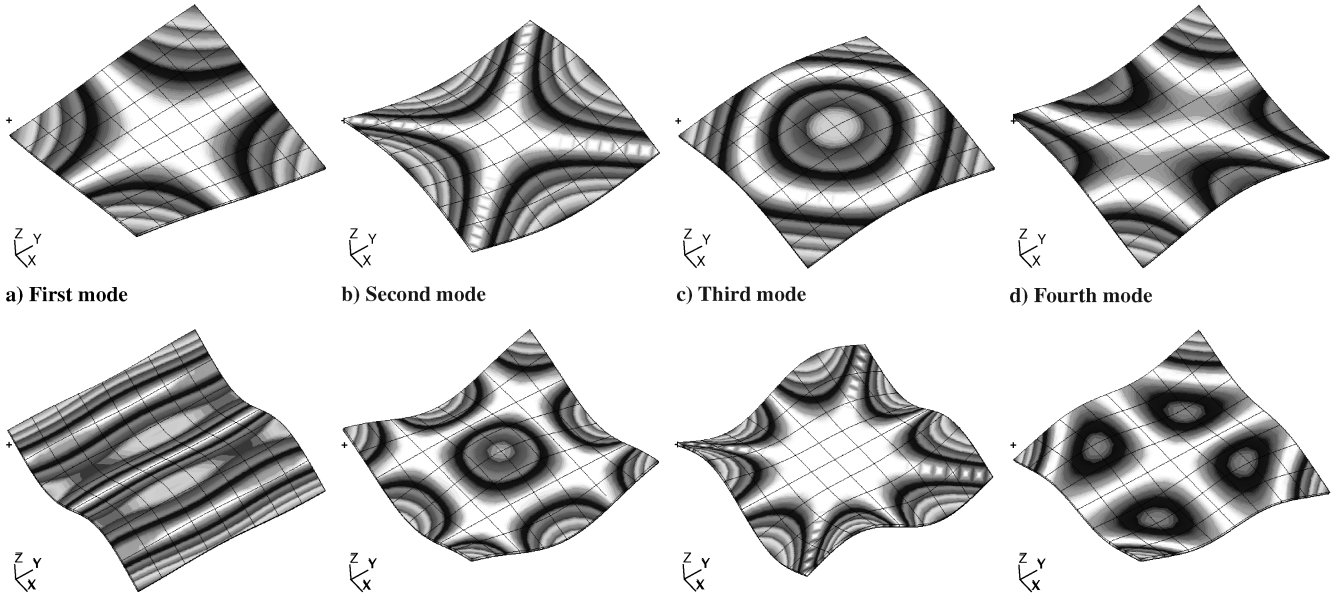

a) First mode b) Second mode c) Third mode d) Fourth mode

e) Fifth mode f) Sixth mode g) Seventh mode h) Eighth mode

Fig. 4 First eight mode shapes of the square plate.

(spatial) frequency modes corresponding to modes three, two, and four, respectively. Among the first five modes, the convergence rate of the solid and shell models are almost the same as for the shear dominated modes, Figs. 5a and 5d. For the bending dominated modes, Figs. 5b, 5c, and 6a, the *p* version has a higher rate of convergence, which increases with higher polynomial orders. Using a seventh-order polynomial expansion, the converged results can be obtained just using one element to mesh the square plate. For the

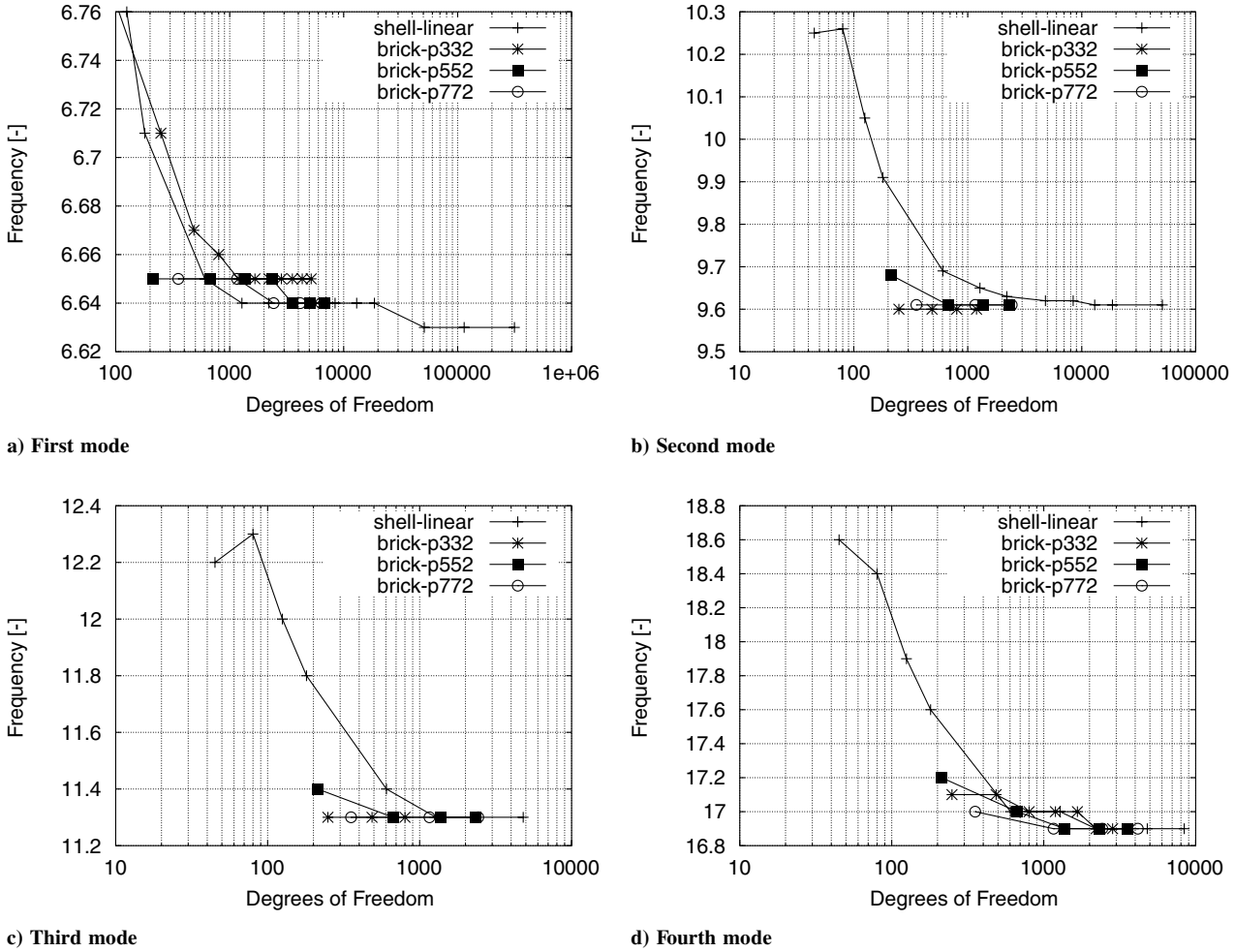

a) First mode b) Second mode

c) Third mode d) Fourth mode

Fig. 5 Comparison of the *h*-convergence histories of the shell and solid models for modes 1–4 of a thick plate.

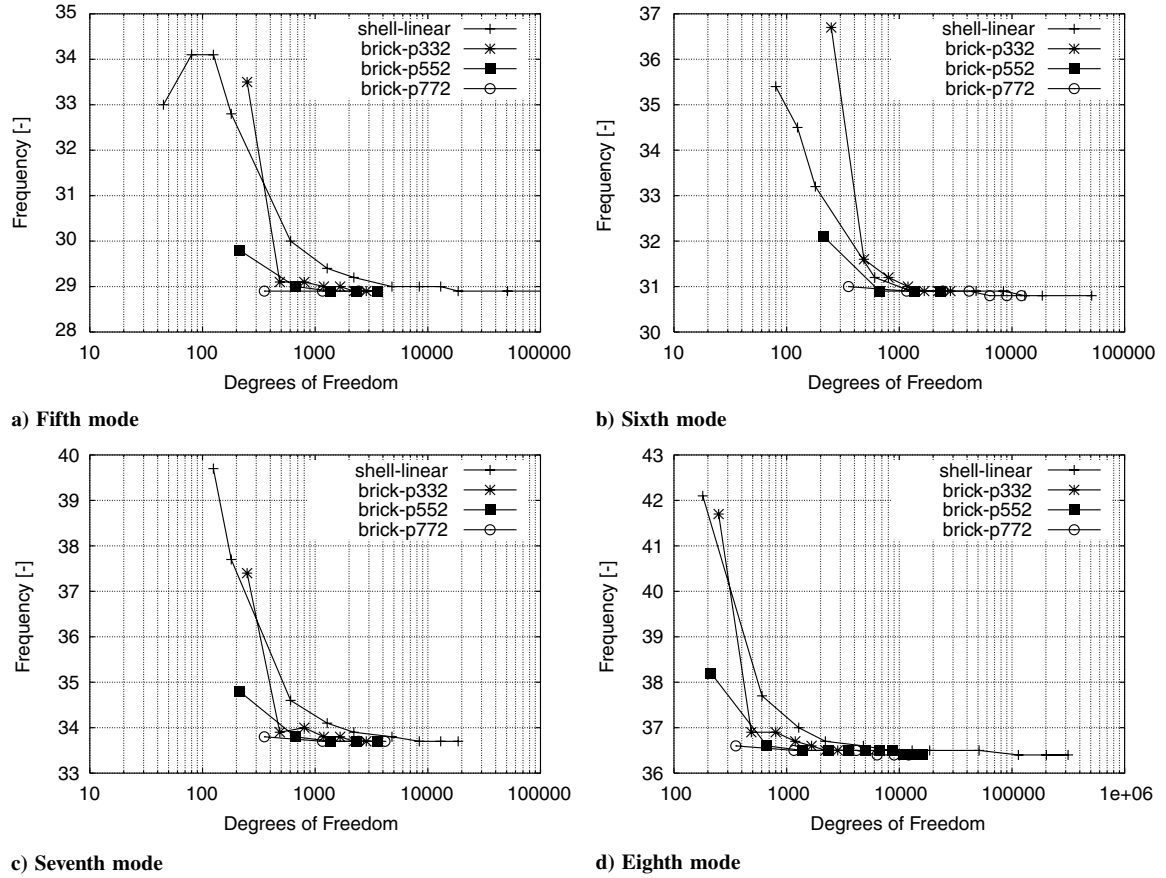

a) Fifth mode

b) Sixth mode

c) Seventh mode

d) Eighth mode

Fig. 6 Comparison of the *h*-convergence histories of the shell and solid models for modes 5–8 of a thick plate.

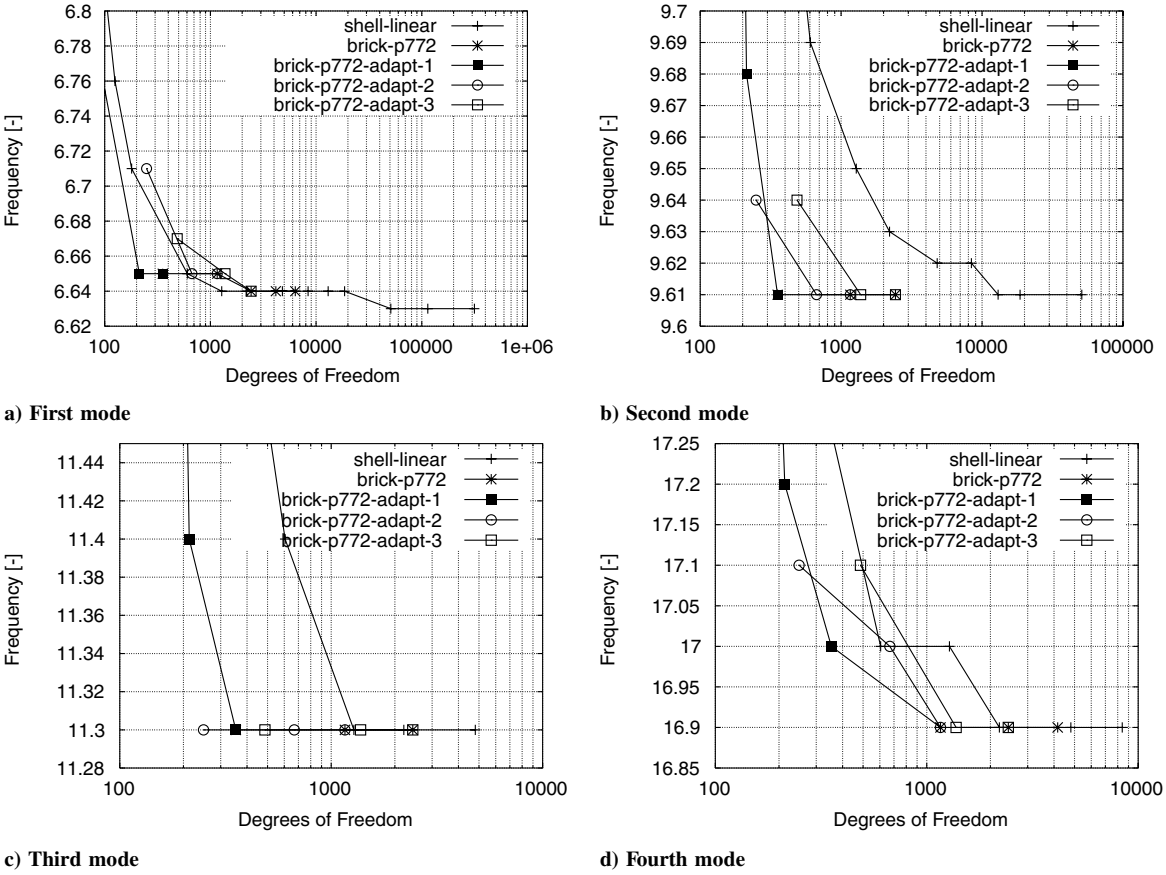

a) First mode

b) Second mode

c) Third mode

d) Fourth mode

Fig. 7 Comparison of the *h*- and *p*-convergence histories of the shell and solid models for modes 1–4 of a thick plate.

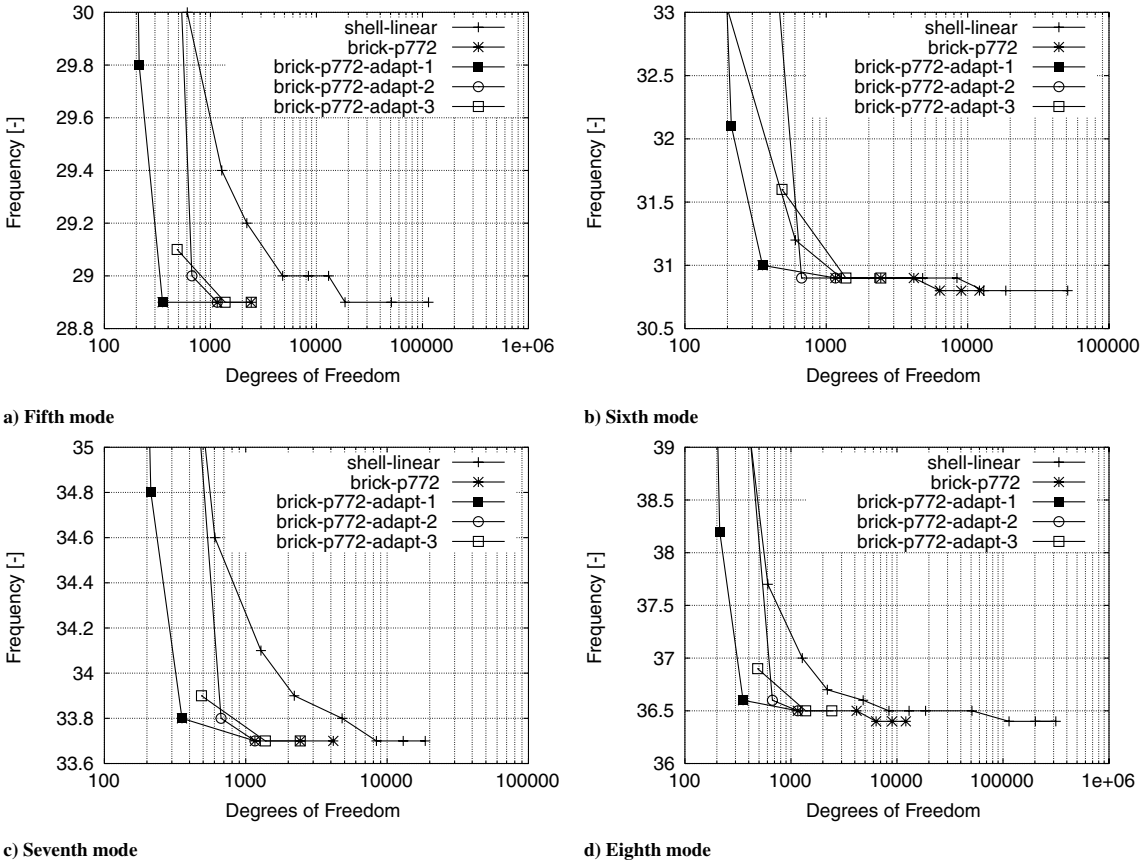

Fig. 8 Comparison of the *h*- and *p*-convergence histories of the shell and solid models for modes 5–8 of a thick plate.

remaining modes, (6–8 of Fig. 4) the convergence rate of the solid models is still higher than the shell model, but an exact match between the converged values of the frequencies can be achieved only by the fifth and seventh polynomial order in some cases.

The traditional approach for the convergence analysis requires the generation of several meshes. Using the *p* elements another approach can be followed: generating one single mesh and increasing the polynomial order until a converged result has been achieved. A comparison between the *standard* and the *polynomial* convergence analysis is performed.

Figures 7 and 8 show the convergence curves for the shell model and the solid model, obtained by increasing the number of elements. In addition, the convergence curves for the solid model performing an adaptive analysis are plotted; in this case, an initial mesh is chosen and then, starting from the second order, the polynomial expansion is increased until the seventh order is reached in the adaptive analysis. Three initial different meshes are chosen, based on one, two, and three elements per (in-plane) edge. The corresponding convergence curves are named respectively brick-p772-adapt-1, brick-p772-adapt-2, and brick-p772-adapt-3. The maximum polynomial order is set to seven, to verify that the result obtained by the adaptive analysis, in which the polynomial order is increased during the analysis, is coincident with the result obtained in the standard way, with a fixed polynomial order (curve named brick-p772). Of course the polynomial order can be raised to any order until convergence is achieved.

For a better comparison of the results, the scale of the figures has been chosen to include frequencies within 10% of the converged value. The figures show that for the first three modes, using just one finite element, a converged result can be obtained with at least the same rate of convergence as the shell model, but using less calculation steps (only three) and with less degrees of freedom. From the fourth mode on, a mesh of $2 \times 2 \times 1$ elements ensures a converged result within a few percent of the converged one just at the second adaptive step. The same accuracy for each of the eight modes can be achieved by using a $3 \times 3 \times 1$ elements mesh, whereas for the shell model the number of calculation steps (each one associated with a completely new mesh generation) is at least six. Moreover, it must be noted that none of the meshes used for the adaptive computations achieve the same converged result of the brick-p772 curve for the "higher order" modes 6–8; nevertheless, the difference is at the third decimal digit.

The comparison of the number of degrees of freedom needed to achieve a solution within a certain accuracy is one method of comparing the performance of the *h* convergence versus the *p* convergence analysis methods. Another way to compare the efficiency of the two methods is the time needed to obtain a converged result. Indeed, there is a big difference in the structure of the stiffness matrix for the shell and the solid models considered here. For a shell model the stiffness matrix is sparse, whereas a solid, *p* formulation model has a full stiffness matrix, which, ceteris paribus, is expected to lead to more computational time.

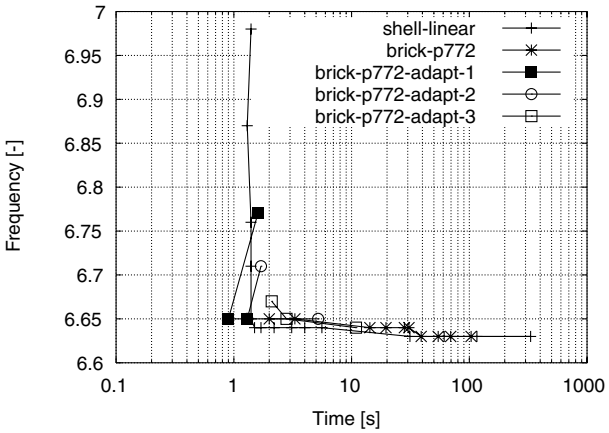

Fig. 9 Comparison of the *h*- and *p*-convergence histories, in terms of CPU time, of the shell and solid models for the first mode of a thick plate.

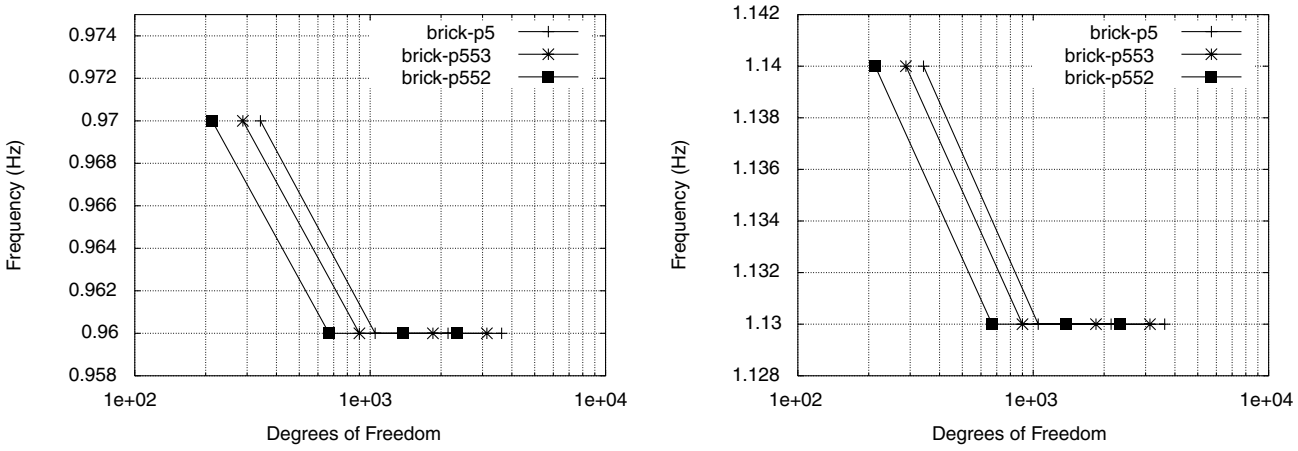

a) Second mode **b) Third mode**

Fig. 10 Sensitivity analysis for the polynomial order choice along the thickness for a thin plate.

Figure 9 reports the convergence history of the first frequency versus the CPU time of each computation for the shell and solid models. The CPU time is available in one of the standard output files of NASTRAN. As can be seen, the solid models require two or three steps of an adaptive analysis to achieve convergence. The time needed by each of these steps is comparable with the time needed by the shell model and in some case is even lower. Even from the CPU-time standpoint, the solid models perform better than the shell model. Nevertheless, it must be considered that such a comparison does not take into account the time needed to regenerate a new mesh for the shell model at each computational step. For the solid model, the CPU time comprises the time needed to evaluate the local convergence of the solid model and to reassign a new set of polynomial orders to the shape functions used by the p elements. Therefore, such a comparison can be used to analyze the differences in the solvers of the eigenvalue problems of the shell and the solid p elements; it cannot be used to make a distinguishing selection between the two different analysis methods when compared with each other.

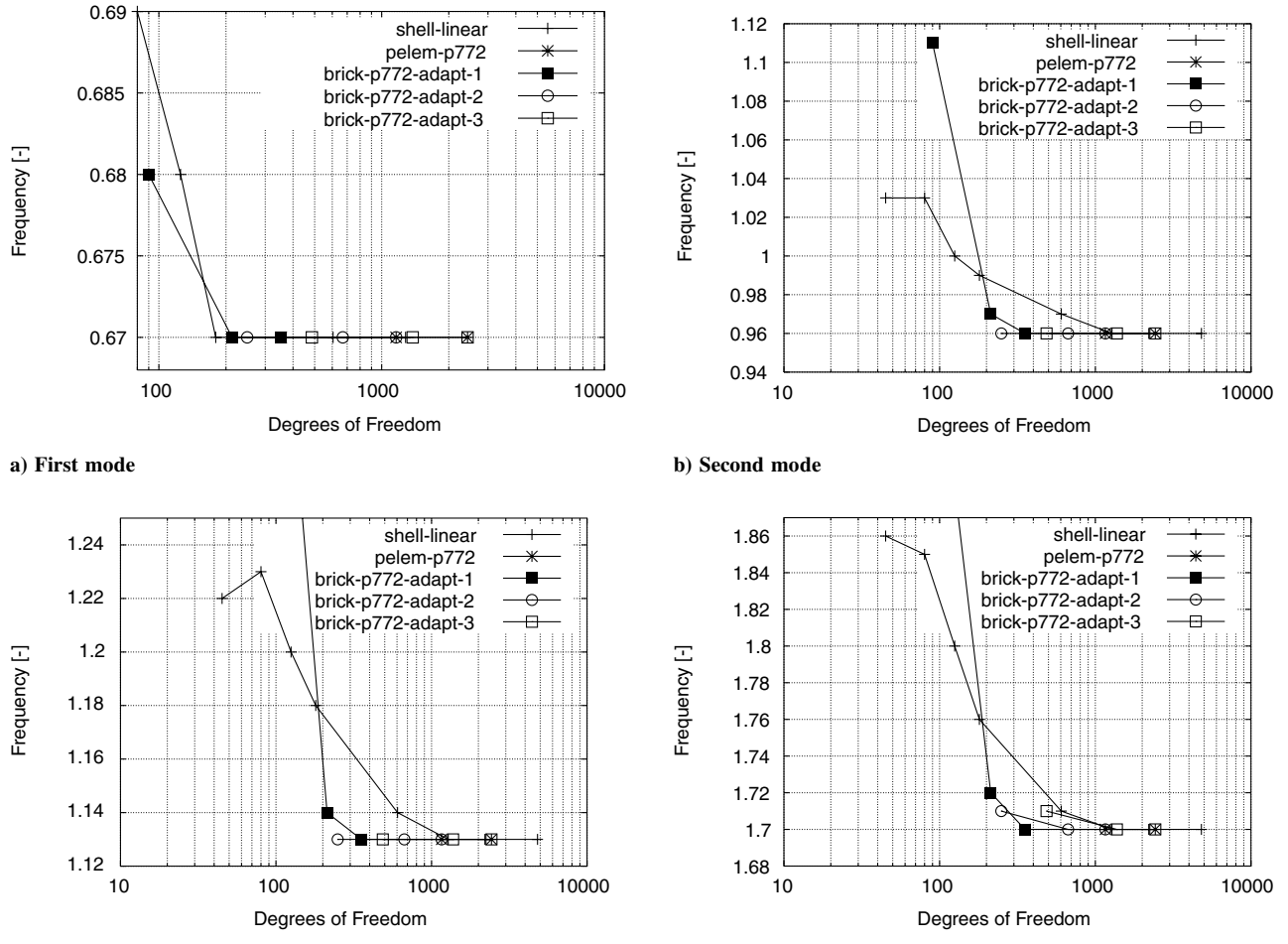

a) First mode **b) Second mode**

c) Third mode **d) Fourth mode**

Fig. 11 Comparison of the h- and p-convergence histories of the shell and solid models for modes 1–4 of a thin plate.

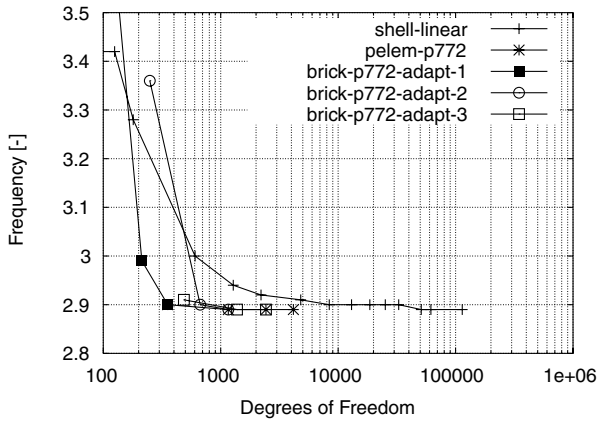

a) Fifth mode

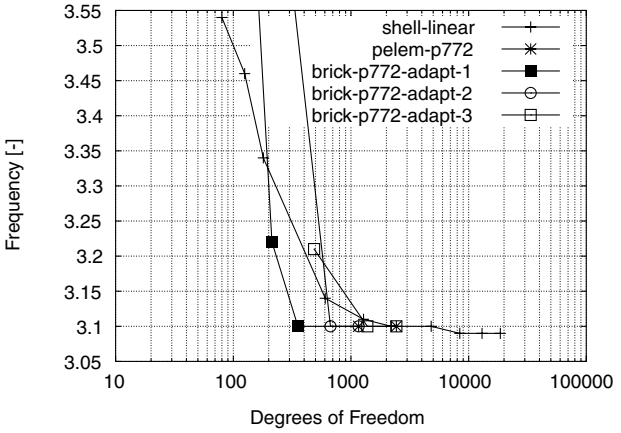

b) Sixth mode

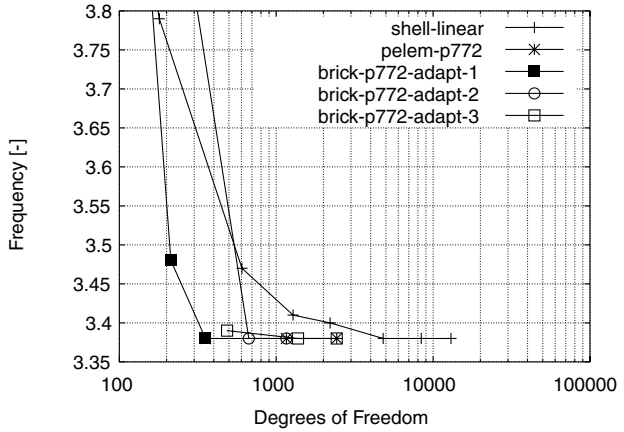

c) Seventh mode

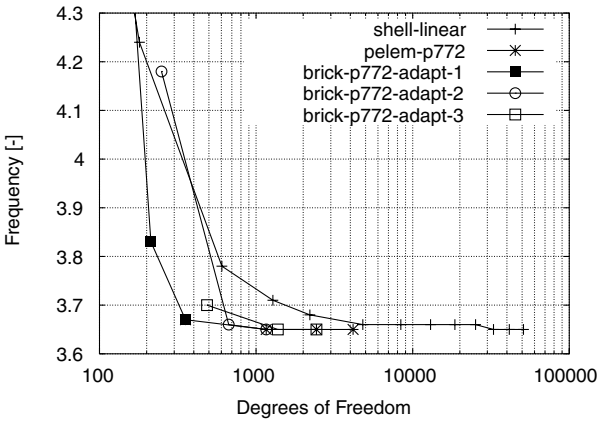

d) Eighth mode

Fig. 12 Comparison of the *h*- and *p*-convergence histories of the shell and solid models for modes 5–8 of a thin plate.

B. Thin Plate

The plate analyzed has dimensions of $L_1 \times L_2 \times L_3 = 1 \times 1 \times 0.001$. The same analyses carried out for the thick plate are performed for this case. For the solid model, only one element will be considered along the thickness and the polynomial order along the thickness can be limited to the second order, as shown in Fig. 10. A comparison between the convergence behavior of the shell model and different solid models is performed. The convergence analysis for the shell model is performed increasing the number of elements, whereas the analysis for the solid model is performed using an adaptive method. Three different initial meshes are chosen, based on one, two, and three elements per edge. The minimum polynomial order chosen is 3 and the maximum is 7. The curves corresponding to the three meshes are referred to in the plots as brick-p772-adapt-1, brick-p772-adapt-2, and brick-p772-adapt-3. Besides the adaptive analysis, a standard analysis is performed for the solid model, increasing the number of elements and keeping the polynomial order fixed to 7. The corresponding curve is referred to in the plots as brick-p772.

The results are reported in Figs. 11 and 12. The adaptive analyses with solid elements show a convergence rate higher than the shell model. For each mode, the number of adaptive analyses needed to achieve convergence varies from three computations for the brick-p772-adapt-1 model up to two computations for the brick-p772-adapt-2 and brick-p772-adapt-3 models, whereas the shell model requires at least five computational steps. Moreover, the shell model requires a number of degrees of freedom higher than the solid models to achieve convergence with the exception of the first mode. This condition is also verified for the nonconverged solutions, starting

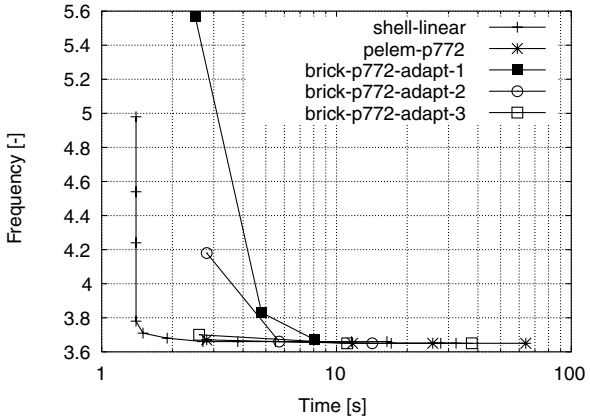

Fig. 13 Comparison of the *h*- and *p*-convergence histories, in terms of CPU time, of the shell and solid models for the eighth mode of a thin plate.

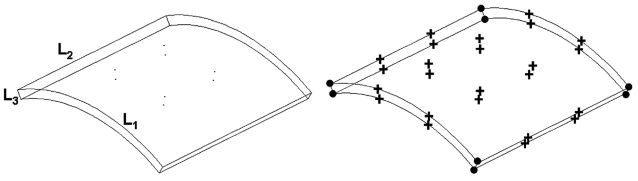

a) Cylindrical panel geometrical parameters

b) One element mesh: corner nodes (point circles) and points for the higher order geometry description (crosses)

Fig. 14 Cylindrical panel geometry and example mesh.

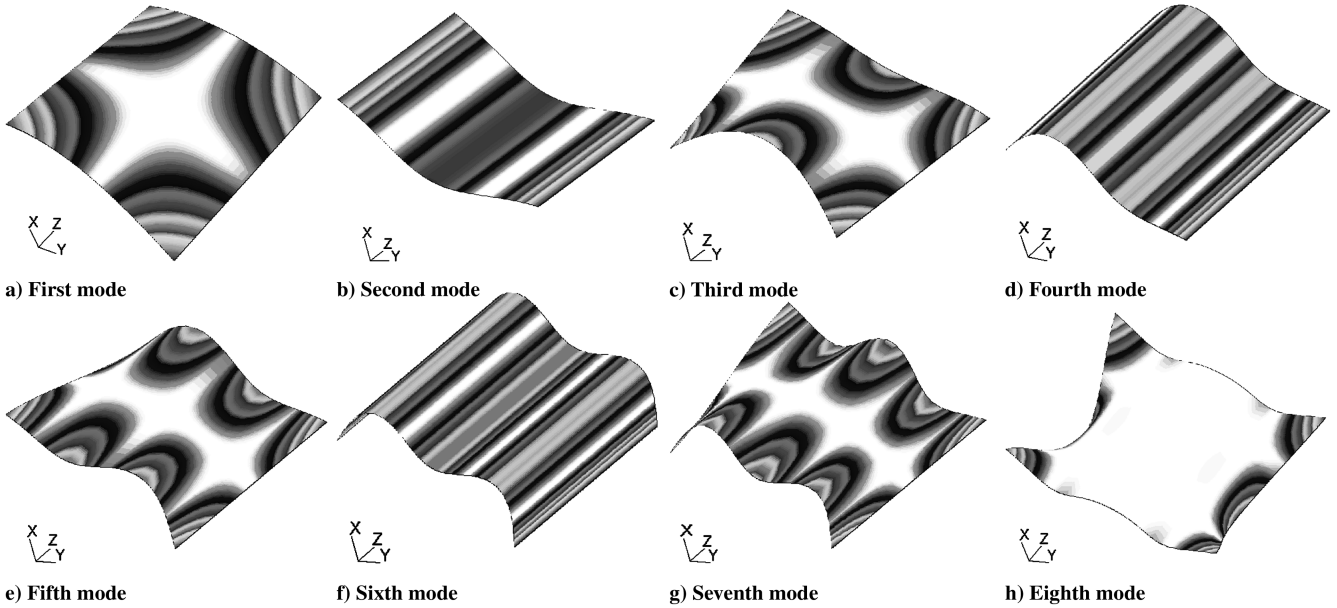

a) First mode b) Second mode c) Third mode d) Fourth mode

e) Fifth mode f) Sixth mode g) Seventh mode h) Eighth mode

Fig. 15 First eight mode shapes of the cylindrical panel.

from the second adaptive computation for each of the solid models considered.

Figure 13 reports the convergence history of the eighth frequency versus the computational time. Unlike the thick plate, the solid models of the thin plate take more time than the shell model considered. This is probably due to the extremely high aspect ratio of the solid elements. This can create difficulties in the solution of the system of linear equations for the determination of the modes and frequencies. Nevertheless, it must be remarked again that the time spent for the regeneration of the different meshes of the shell model

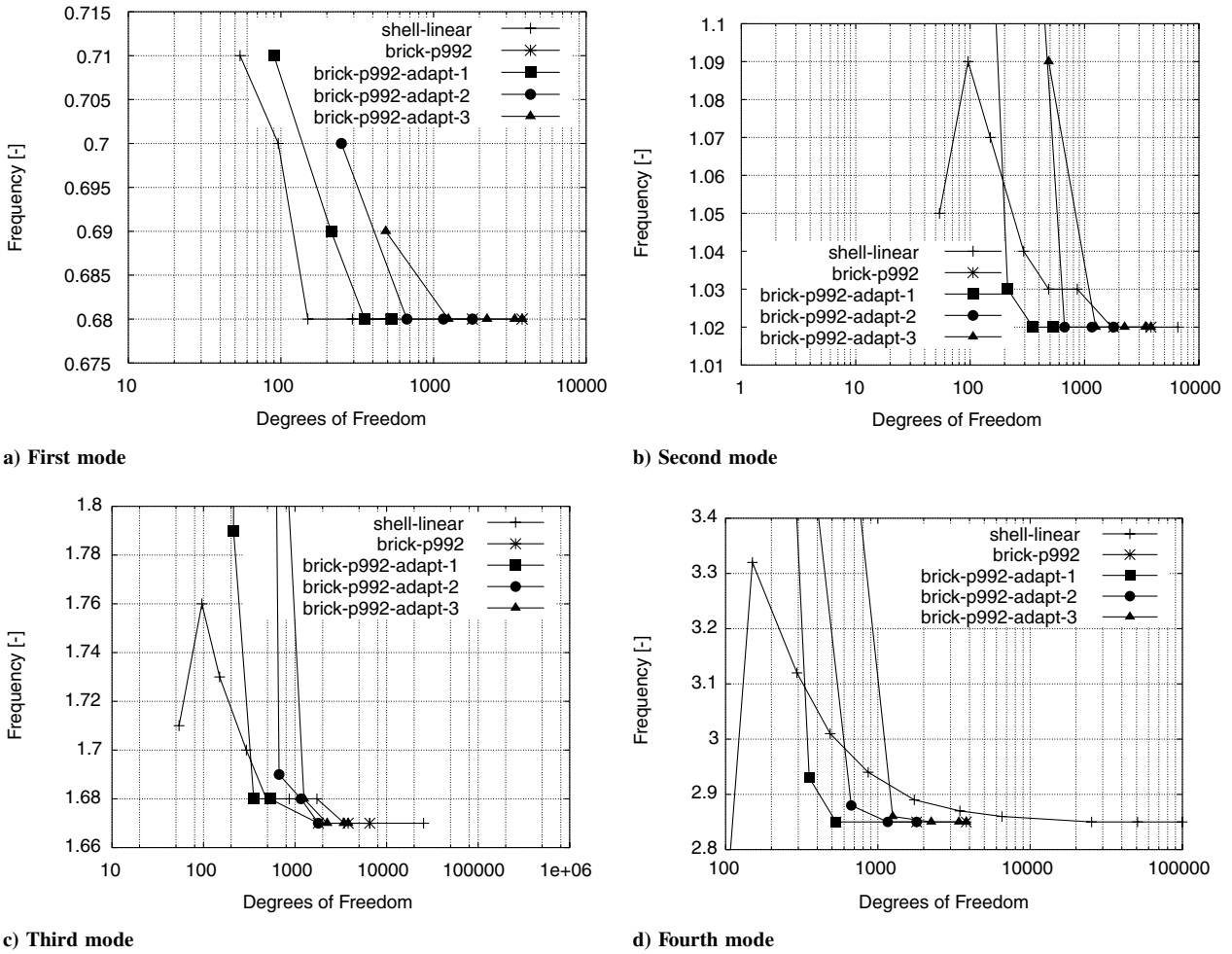

a) First mode b) Second mode

c) Third mode d) Fourth mode

Fig. 16 Comparison of the *h*- and *p*-convergence histories of the shell and solid models for modes 1–4 of a cylindrical panel.

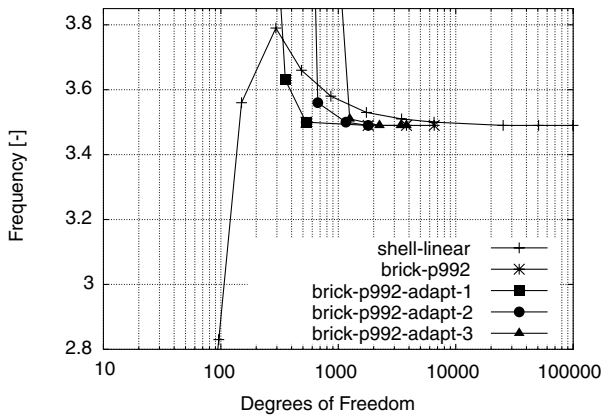

a) Fifth mode

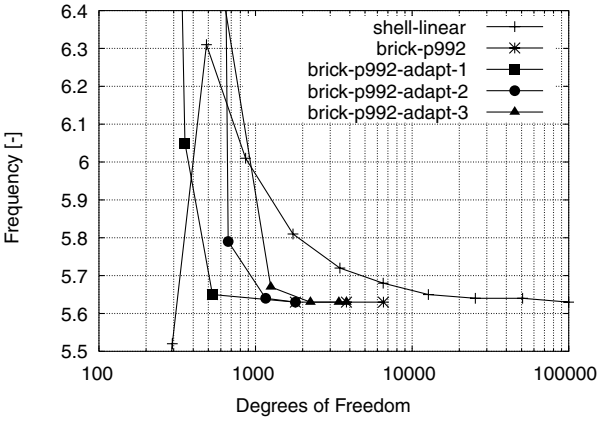

b) Sixth mode

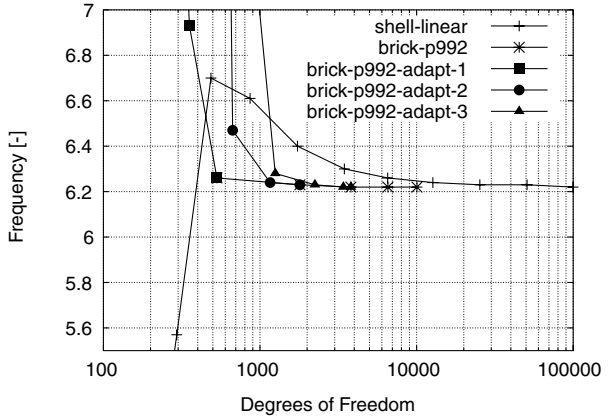

c) Seventh mode

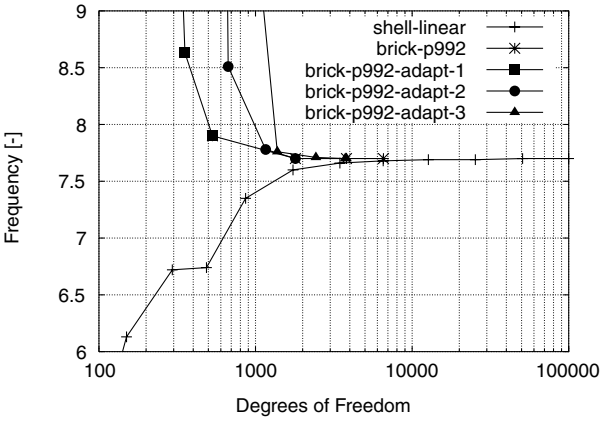

d) Eighth mode

Fig. 17 Comparison of the *h*- and *p*-convergence histories of the shell and solid models for modes 5–8 of a cylindrical panel.

are not taken into account, whereas the CPU time of the solid models includes the time spent for the regeneration of the polynomial order to the FE model. Therefore, the comparison is still related to the particular eigenvalue problem solver and not to the convergence process itself.

IV. Modal Analysis of Curved Panels

In the standard approach of the finite-element method, the mesh refinement guarantees that the geometry is approximated more and more accurately. In particular, the shape functions describing the unknown displacement field are also used to describe the geometry, and the finite element is referred as *isoparametric*. At the limit, when the reference size of the largest element tends to be zero, the representation of the domain is exact. In the *p* version of the finite-element method, the mesh, rather coarse, is left unchanged and convergence is achieved by increasing the order of the polynomial order of the shape functions. Therefore, it is important that the geometry of the structure is accurately modeled given the small amount of elements used. Different methods have been developed to describe complex geometries with few elements, one of the most popular is the so-called blending functions method, from Gordon and Hall [13]. In this case, the mapping from the local coordinates to the global, Cartesian coordinates of the element is made of the standard (linear) mapping of isoparametric elements and two additional mappings consisting of a face and an edge blending [6]. The additional mappings provide a higher order representation for the geometry of the element.

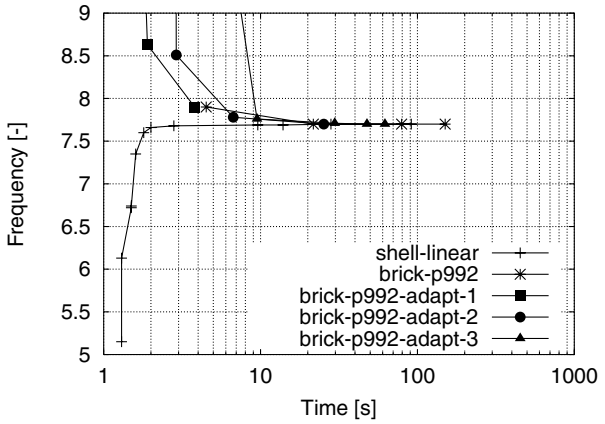

Fig. 18 Comparison of the *h*- and *p*-convergence histories, in terms of CPU time, of the shell and solid models for the eighth mode of a cylindrical panel.

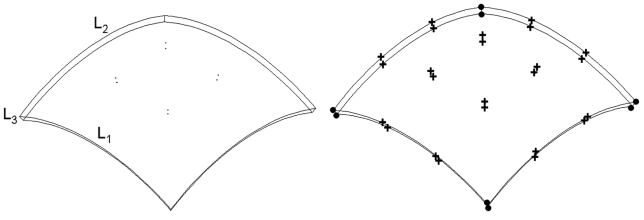

a) Spherical panel geometrical parameters

b) One element mesh with corner nodes and point for the higher order geometry description (crosses)

Fig. 19 Spherical panel geometry and example mesh.

In NASTRAN the curved edges of finite elements are described as rational parametric cubic curves [14] and the faces are defined as rational parametric bicubic surfaces [14]. To have such a description for each curved surface of the finite elements, sixteen additional points, equally spaced in the two parametric coordinates of the surface, must be specified in the input file. The points lying on each edge are also moved so as to maintain C^1 continuity of adjacent edges.

A. Thin Cylindrical Panel

The mean surface of the panel has dimensions of $L_1 \times L_2 \times L_3 = 1 \times 1 \times 0.001$, Fig. 14. A finite-element model is created using linear shell elements. Several modal analyses are performed, generating several meshes. Each new analysis is performed, doubling the number of elements. A solid model is then generated. A standard convergence analysis is performed, increasing the number of elements along the in-plane edges, whereas along the thickness the number of elements is fixed to one and the polynomial order is kept constant. An adaptive analysis is then performed considering three different meshes having one, two, and three elements per (in-plane) edge. Mode shapes are reported in Fig. 15.

The polynomial order starts from 3 up to 9 along the in-plane edges, whereas along the thickness the order is kept to 2. The comparison of the different results is reported in Figs. 16 and 17, where the curves corresponding to the three adaptive analyses are referred to as brick-p992-adapt-1, brick-p992-adapt-2, and brick-p992-adapt-3. For the pure shear mode, Figs. 16a and 15a, the shell model reaches a converged value with less degrees of freedom, whereas for the other modes the solid models exhibit a higher convergence rate and attain a converged value with less degrees of freedom. The higher convergence rate is exhibited by the bending dominated modes, Figs. 15b, 15d, 15f, 16b, 16d, and 17b. For the adaptive analysis made with solids, two or three computations are sufficient to get converged results, whereas for the shell model, the number of computations is almost double.

Finally, Fig. 18 reports the convergence history of the eighth frequency versus the CPU time. In terms of converged values, the solid models require less computational time (sum of all the CPU times corresponding to each point of a curve). Conversely, if the convergence process is stopped when the difference between two successive computations is relaxed to be a few percent from each other, then the shell model requires less time than the solid models (especially the brick-p992-adapt-2, and brick-p992-adapt-3). On the other hand, the shell model requires more computational steps than the solid models and therefore more time for interfacing operations such as mesh regeneration.

B. Thin Spherical Panel

The mean surface of the panel analyzed has dimensions of $L_1 \times L_2 \times L_3 = 1 \times 1 \times 0.001$, Fig. 19. A comparison between the convergence behavior of the shell model and different solid models is performed. The convergence analysis for the shell model is performed by doubling the number of elements for each run, whereas the analysis for the solid model is performed using an adaptive method with a constant number of elements. Three different initial meshes are chosen, based on two, three, and four elements per edge. The minimum polynomial order chosen is 3 and the maximum is 12, as due to the double curvature the convergence rate is expected to be slower. One element is taken along the thickness. Mode shapes are reported in Fig. 20.

The curves corresponding to the three solid meshes are referred to in the plots as brick-p12122-adapt-2, brick-p12122-adapt-3, and brick-p12122-adapt-4. Besides the adaptive analysis, a standard analysis is performed for the solid model, increasing the number of elements and keeping the polynomial order fixed to 12. The corresponding curve is referred to in the plots as brick-p12122.

The results are reported in Figs. 21 and 22. The adaptive analyses with solid elements exhibits a convergence rate higher than the shell models, but in this case the converged value is slightly different depending on the initial mesh used, so in this case the solid formulation needs elements with an aspect ratio lower than a single curvature or a flat panel. The converged value is achieved using about the same number of degrees of freedom of the shell model, except for the first, pure shear mode, in which the shell model performs better than the solid ones. In any case, the number of calculation steps required by the shell model is almost double the number of computations for the solid model, and for each computation a new mesh must be generated. This is easy for a simple panel; it is practically not affordable for a more complex model, like a wing structure.

Figure 23 reports the convergence history of the shell and solid models as a function of the CPU time. In this case, the shell models perform better than the solid modes, both in terms of the fully converged solution and in terms of a solution within a few percent of the converged value. Moreover the *h*-convergence analysis performed with the solid model oscillates without reaching a fully converged value for the meshes considered in the analysis. Probably the curvature effects due to the geometry of the panel have an effect

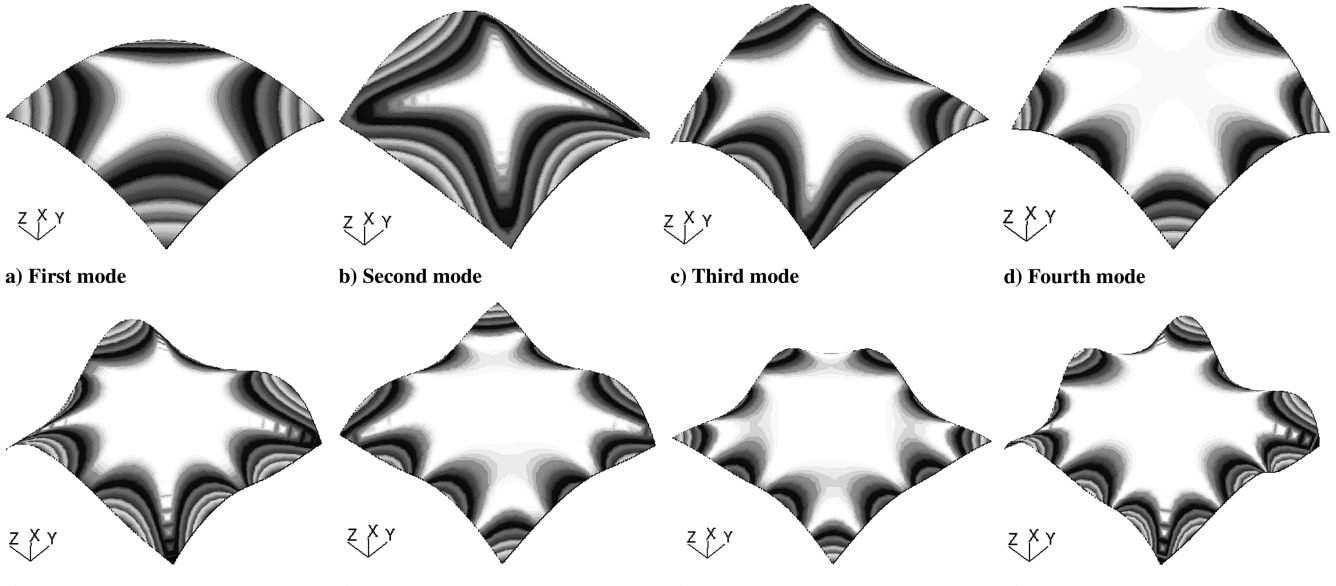

Fig. 20 First eight mode shapes of the spherical panel.

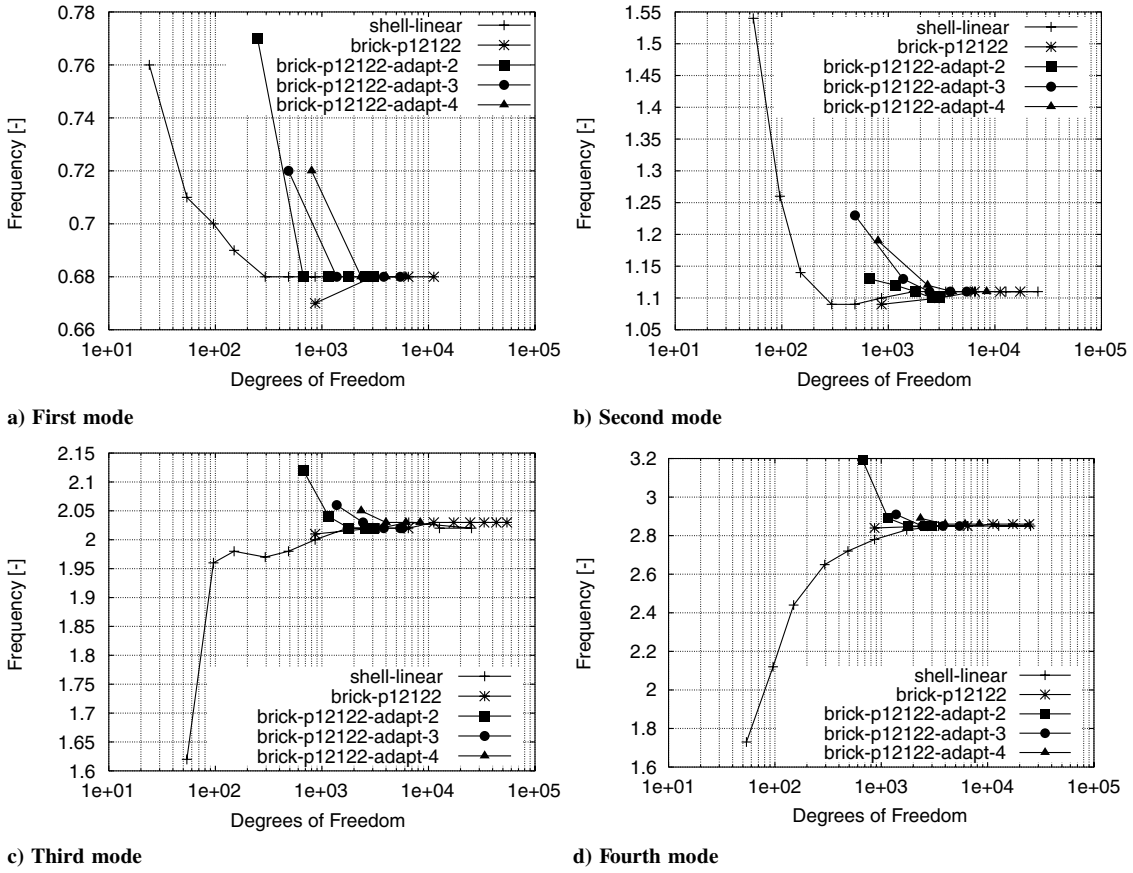

a) First mode

b) Second mode

c) Third mode

d) Fourth mode

Fig. 21 Comparison of the *h*- and *p*-convergence histories of the shell and solid models for modes 1–4 of a spherical panel.

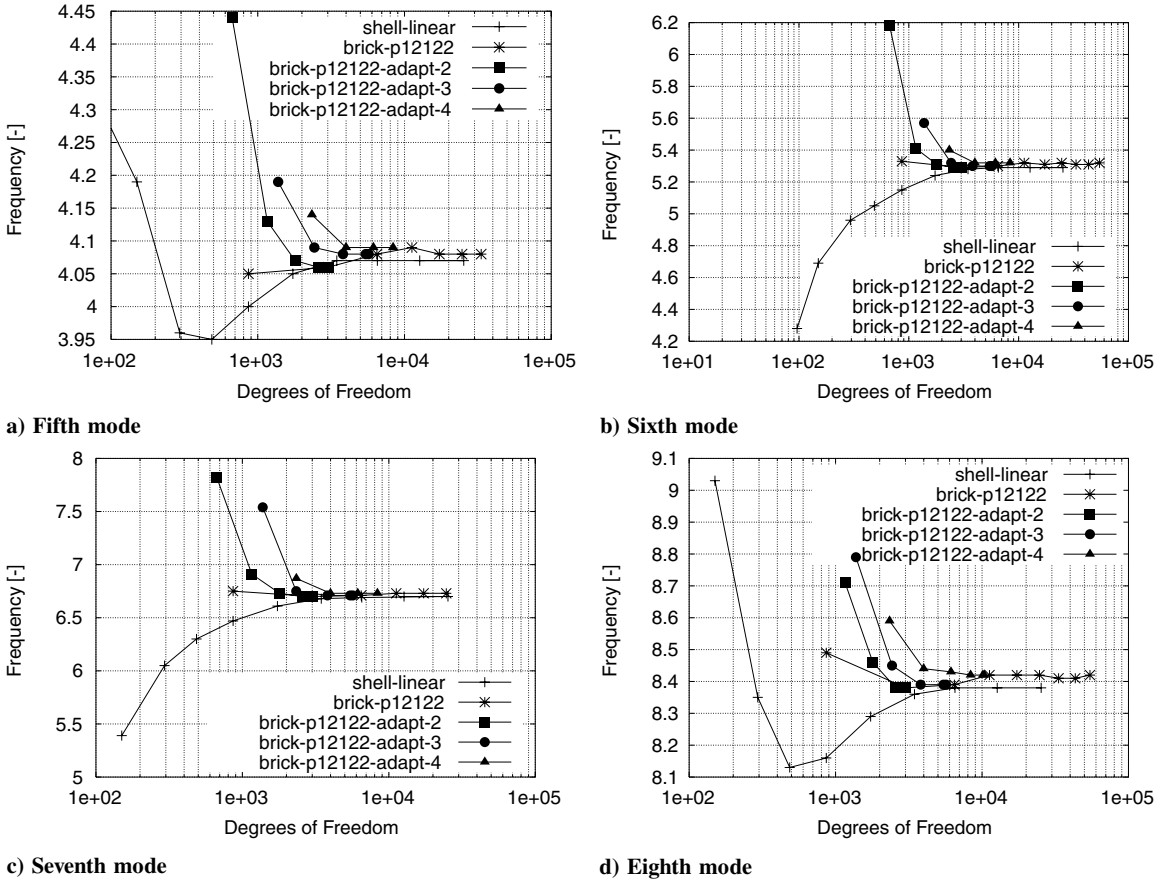

a) Fifth mode

b) Sixth mode

c) Seventh mode

d) Eighth mode

Fig. 22 Comparison of the *h*- and *p*-convergence histories of the shell and solid models for modes 5–8 of a spherical panel.

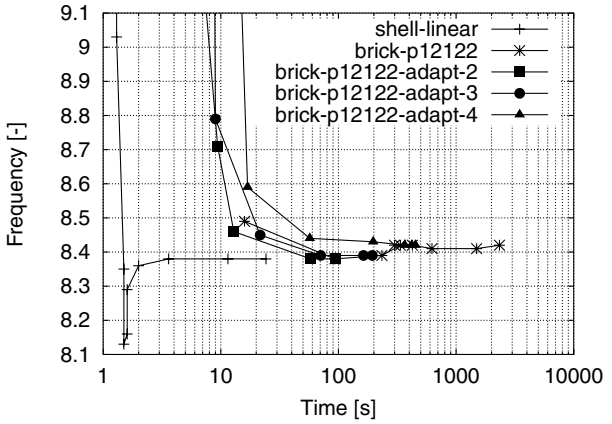

Fig. 23 Comparison of the *h*- and *p*-convergence histories, in terms of CPU time, of the shell and solid models for the eighth mode of a spherical panel.

on the solution of the system of equation that governs the eigenvalue problem.

C. Mass Matrix Formulation

For all the comparisons shown so far, the solid and shell models use a consistent mass matrix formulation, which results in a full mass matrix. Instead, it is industry practice to employ a lumped mass matrix formulation for the shell models, resulting in a diagonal mass matrix. This eases the distribution of the nonstructural masses over, for example, a wing structure, as the nonstructural masses are defined as point masses concentrated in certain nodes.

The *p* formulation of the finite elements instead uses a consistent mass matrix formulation. The mass matrix is full and, in this case, it is difficult to evaluate the cross coupling defined by a concentrated mass.

The choice between a consistent or a lumped mass matrix for a shell model also has an effect on the convergence rate of the natural frequencies. Figures 24 and 25 report the convergence analysis for the double curvature panel analyzed before. A shell model based on both lumped and consistent mass matrices is created as well as a solid model. Convergence is achieved by doubling the number of elements for the shell model, whereas for the solid model an adaptive analysis is performed based on a fixed mesh with three elements per in-plane edge and one along the thickness.

The figure shows that the lumped mass model requires more computations to achieve convergence than the consistent mass model. Besides, for a fixed number of degrees of freedom the results can be much farther from the converged solution than the consistent mass model. The solid model shows its better behavior as few computations are needed to achieve convergence.

V. Conclusions

The results presented so far show how solid, *p*-version finite elements can be used efficiently to model basic kinds of thin walled panels, obtaining the same results as a traditional shell model without any problem in modelling and analyzing very thin structural elements with solids.

Indeed, in all of the cases examined a converged result is achieved using less computational steps (i.e., the number of adaptive

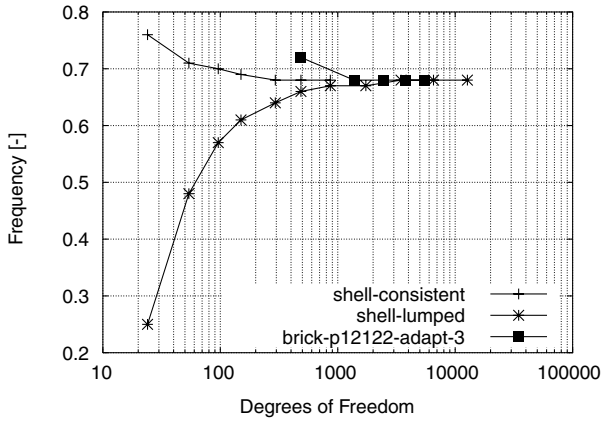

a) First mode

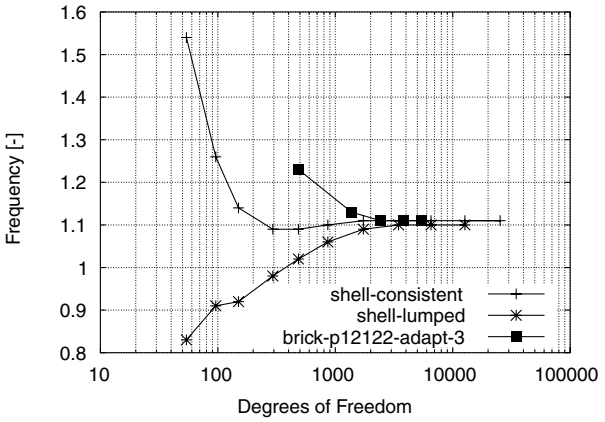

b) Second mode

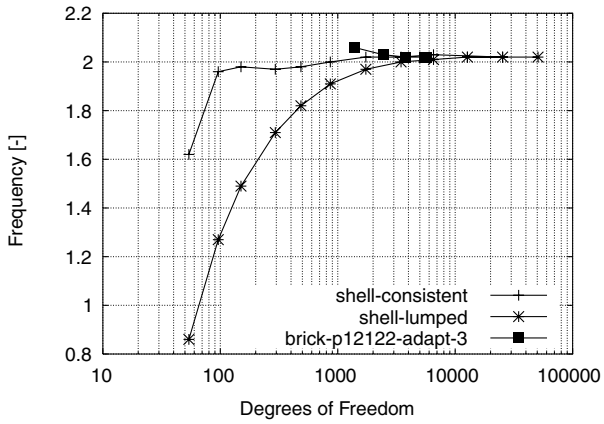

c) Third mode

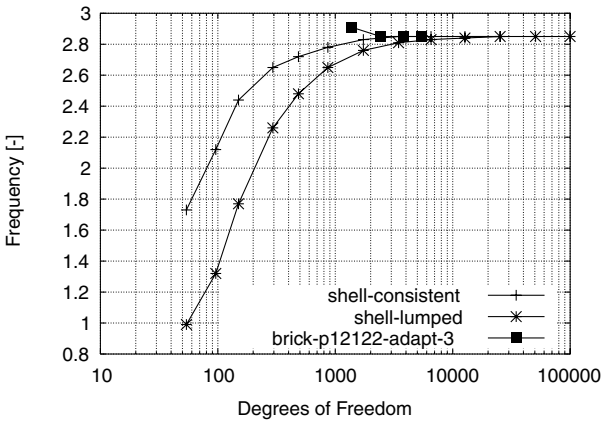

d) Fourth mode

Fig. 24 Effects of the mass matrix formulation, lumped and consistent, on the convergence histories of the shell model for modes 1–4 of a spherical panel.

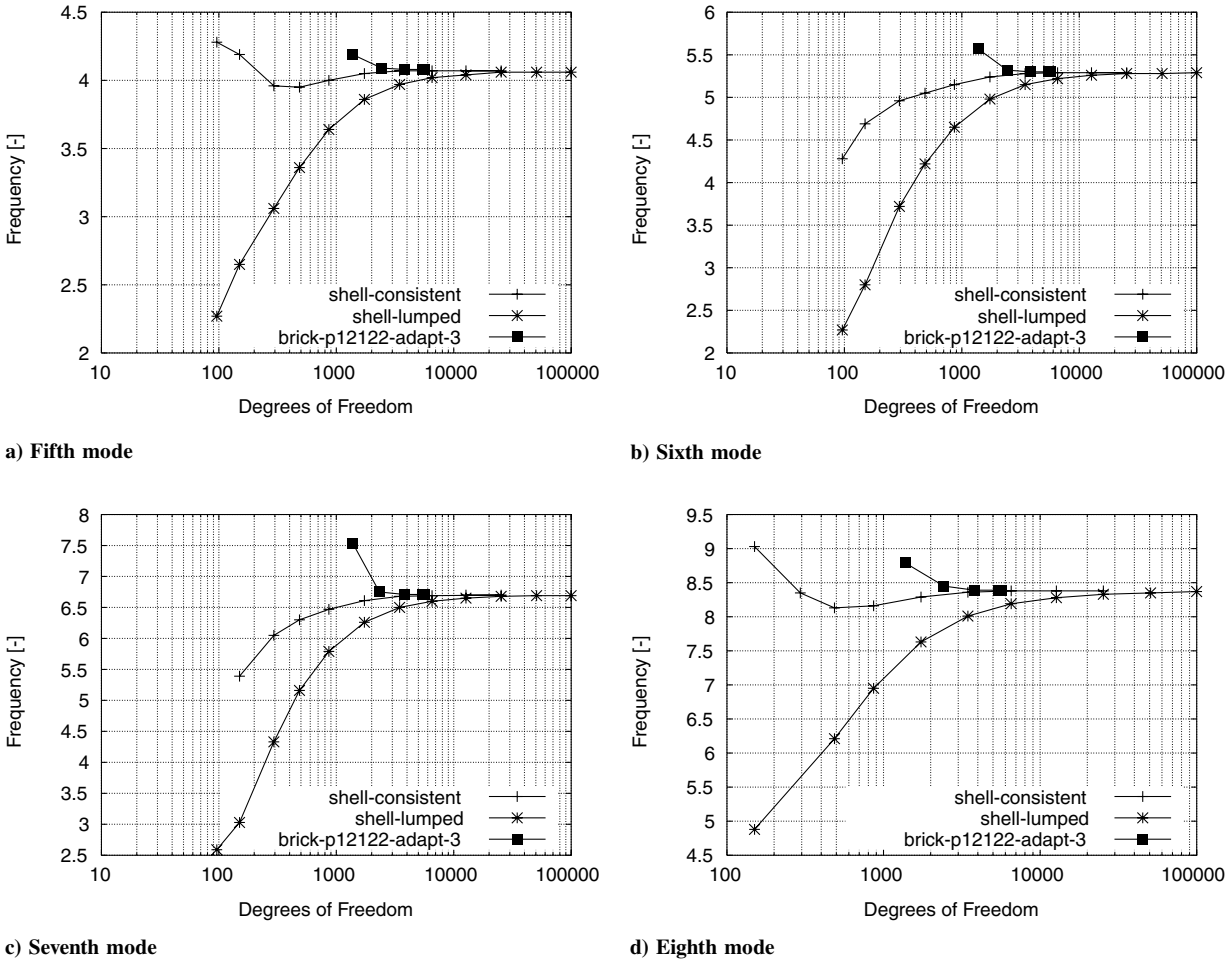

a) Fifth mode

b) Sixth mode

c) Seventh mode

d) Eighth mode

Fig. 25 Effects of the mass matrix formulation, lumped and consistent, on the convergence histories of the shell model for modes 5–8 of a spherical panel.

calculations for the solids and the number of mesh refinements for the shells), and in most of the cases using less degrees of freedom.

The fact that the shell model sometimes predicts better the shear dominated modes is probably due to the fact that the shell model contains as degrees of freedom the rotations, whereas the solid model has only the translations, and the rotations are derived quantities, and so less accurate.

Moreover, a comparison between the shell and the solid models has been also performed in terms of the CPU time required to calculate a solution. For curved panels, that is, cylindrical and spherical panels, the computations of a shell model seemed to be faster than that of a solid model. It must be remarked that a "fair" comparison between the two models should take into account the time needed by the shell model to regenerate a mesh between two successive computations. This time could be much higher than the time needed to compute a solution especially if the remeshing operations are performed by hand or when performed on more complex geometries such as a wing. The *p* formulation, by avoiding the need for mesh regeneration, makes the whole convergence process much more flexible and feasible even for complex structures like a complete aircraft.

References

[1] Babuska, I., Szab'o, B., and Katz, I., "The P-Version of the Finite Element Method," *SIAM Journal on Numerical Analysis*, Vol. 18, No. 3, 1981, pp. 515–545. doi:10.1137/0718033

[2] Timoshenko, S. P., and Woinowsky-Krieger, S., *Theory of Plates and Shells*, 2nd ed., McGraw–Hill, New York, 1959.

[3] Szabo, B., and Sahrmann, G., "Hierarchic Plate and Shell Models Based on P-Extension," *International Journal for Numerical Methods in Engineering*, Vol. 26, No. 8, 1988, pp. 1855–1881. doi:10.1002/nme.1620260812

[4] Babuska, I., and Suri, M., "Locking Effects in the Finite Element Approximation of Elasticity Problems," *Numerische Mathematik*, Vol. 62, No. 1, 1992, pp. 439–463. doi:10.1007/BF01396238

[5] Babuska, I., and Suri, M., "On Locking and Robustness in the Finite Element Method," *SIAM Journal on Numerical Analysis*, Vol. 29, No. 5, 1992, pp. 1261–1293. doi:10.1137/0729075

[6] Düster, A., "High Order Finite Elements for Three Dimensional, Thin-Walled Nonlinear Continua," Ph.D. Dissertation, Technische Universität München—Lehrstuhl für Bauinformatik, June 2001.

[7] Hughes, T. J. R., *The Finite Element Method: Linear Static and Dynamic Finite Element Analysis*, Prentice–Hall, Upper Saddle River, NJ, 1987; reprint, Dover, New York, 2000.

[8] Morino, L., Mastroddi, F., Bernardini, G., and Piccirilli, M., "A Hermite Interpolation Finite Element for Structural Dynamics," *XVI Congresso Nazionale AIDAA*, Associazione Italiana di Aeronautica e Astronautica, Palermo, Italy, Sept. 2001.

[9] MSC NASTRAN Encyclopedia, Ver. 70.5, The MacNeal–Schwendler Corporation, Santa Ana, CA, 1988.

[10] Akin, J. E., *Finite Element Analysis with Error Estimators*, 1st ed., Butterworth–Heinemann, Amsterdam, The Netherlands, 2005, Chap. 5.

[11] Szab'o, B., and Babuska, I., *Finite Element Analysis*, Wiley, New York, 1991.

[12] Cerulli, C., "Un Metodo Agli Elementi Finiti rer Piastre E Gusci Basato Sulla Interpolazione di Hermite," M.S., Universitá Degli Studi di Roma "La Sapienza," May 2001.

[13] Gordon, W. J., and Hall, C. A., "Transfinite Element Methods: Blending Function Interpolation over Arbitrary Curved Element Domains," *Numerische Mathematik*, Vol. 21, No. 2, 1973, pp. 109–129. doi:10.1007/BF01436298

[14] Mortenson, M. E., *Geometric Modeling*, Wiley, New York, 1997, pp. 184–186, Chap. 7.